



HAL
open science

Effects of eddy-driven subduction on ocean biological carbon pump

Laure Resplandy, Marina Lévy, Dennis J. McGillicuddy

► **To cite this version:**

Laure Resplandy, Marina Lévy, Dennis J. McGillicuddy. Effects of eddy-driven subduction on ocean biological carbon pump. *Global Biogeochemical Cycles*, 2019, 33 (8), pp.1071-1084. 10.1029/2018GB006125 . hal-02352097

HAL Id: hal-02352097

<https://hal.science/hal-02352097v1>

Submitted on 1 Dec 2020

HAL is a multi-disciplinary open access archive for the deposit and dissemination of scientific research documents, whether they are published or not. The documents may come from teaching and research institutions in France or abroad, or from public or private research centers.

L'archive ouverte pluridisciplinaire **HAL**, est destinée au dépôt et à la diffusion de documents scientifiques de niveau recherche, publiés ou non, émanant des établissements d'enseignement et de recherche français ou étrangers, des laboratoires publics ou privés.

Effects of eddy-driven subduction on ocean biological carbon pump

Laure Resplandy¹, Marina Lévy², Dennis J. McGillicuddy Jr.³

¹Princeton University, Geosciences Department, Princeton Environmental Institute, Princeton, NJ 08544, USA.

²Sorbonne Université, CNRS, IRD, MNHN, LOCEAN-IPSL, Paris, France

³Woods Hole Oceanographic Institution, Department of Applied Ocean Physics and Engineering, Woods Hole, MA 02543, USA.

Key Points:

- A high-resolution model simulates realistic hotspots of organic carbon export by physical subduction.
- Eddy-driven subduction contributes little to annual export due to compensation between upward and downward fluxes.
- Eddy-driven spatio-temporal variations in the mixed-layer efficiently export dissolved and particulate organic carbon.

Abstract

Estimates of the ocean biological carbon pump are limited by uncertainties in the magnitude of the physical injection of particulate (POC) and dissolved (DOC) organic carbon to the ocean interior. A major challenge is to evaluate the contribution of these physical pumps at small spatial and temporal scales (< 100 km and < 1 month). Here, we use a submesoscale permitting bio-physical model covering a large domain representative of a subpolar and a subtropical gyre to quantify the impact of small-scale physical carbon pumps. The model successfully simulates intense eddy-driven subduction hotspots with a magnitude comparable to what has been observed in nature ($1000\text{-}6000$ mgC m⁻² d⁻¹). These eddy-driven subduction events are able to transfer carbon below the mixed-layer, down to 500-1000 m depth. However, they contribute $< 5\%$ to the annual flux at the scale of the basin, due to strong compensation between upward and downward fluxes. The model also simulates hotspots of export associated with small-scale heterogeneity of the mixed-layer, which intermittently export large amounts of suspended POC and DOC. The mixed-layer pump contributes $\sim 20\%$ to the annual flux. High resolution measurements of export flux are needed to test models such as this one, and to improve our mechanistic understanding of the biological pump and how it will respond to climate change.

1 Introduction

The oceanic biological carbon pump draws down atmospheric CO₂ by exporting particulate and dissolved organic carbon (POC and DOC) produced at the surface by marine ecosystems to the deep ocean (Falkowski et al., 1998). Estimates of the global carbon export associated with the biological pump vary widely between 5 and 15 Gt y⁻¹ (Siegel et al., 2014; Henson et al., 2011, 2012; Boyd & Trull, 2007; Dunne et al., 2007; Schlitzer, 2004; Laws et al., 2000; DeVries & Weber, 2017; Boyd et al., 2019). Achieving a better constraint on the magnitude of the biological pump is difficult because it requires the characterization of multiple biological and physical processes that transfer and transform organic carbon. A particularly daunting challenge is to quantify the impact of processes occurring at small spatial and temporal scales (scales < 100 km and < 10 days) on the export flux at annual and large spatial scales ($\mathcal{O}1000$ km).

At large spatial scale, the export is dominated by the passive sinking of POC produced in the well lit surface layer or euphotic zone - referred to as the *gravitational pump*. Two physical processes complement the gravitational pump: the deepening of the mixed-layer that carries organic carbon out of the euphotic zone and leaves it behind during restratification - referred as the *mixed-layer pump* and Ekman pumping of organic carbon associated with wind driven ocean circulation - referred as the *Ekman pump*. Globally, the gravitational pump is estimated to be 4 to 9 PgC/y (Bopp et al., 2013; Siegel et al., 2014; DeVries & Weber, 2017; Boyd et al., 2019) and the mixed-layer pump around 2.0-2.4 PgC/y (corresponding to annual exports of 1.9 Pg of DOC and 0.1-0.5 Pg of POC, Hansell et al., 2009; Dall’Olmo et al., 2016)). The Ekman pump is considered to be weaker and around 0.7 PgC/y because of compensation between regions of downward and upward Ekman pumping (Lévy et al., 2013).

Fine scale measurements have, however, revealed that POC export can be intensified at the center of ocean mesoscale eddies or in frontal structures at their periphery (Newton et al., 1994; McGillicuddy et al., 2007; Benitez-Nelson et al., 2007; Buesseler et al., 2009; Guidi et al., 2012; Estapa et al., 2015; Omand et al., 2015; Waite et al., 2016; Stukel, Aluwihare, et al., 2017; Stukel, Song, et al., 2017). Observations have also highlighted the presence of localized maxima in POC concentrations below the base of the euphotic layer, which are interpreted as evidence of small-scale physical subduction of POC (Omand et al., 2015; Stukel, Aluwihare, et al., 2017; Llort et al.,

2018). High resolution bio-physical models suggest that these subduction "hotspots" are sustained by intense downward vertical velocities of the order of 1-100 m d⁻¹ that can locally subduct POC (Lévy et al., 2001; Karleskind et al., 2011; Omand et al., 2015). These ageostrophic velocities ensue both from mesoscale dynamics and sub-mesoscale frontal dynamics. Here we will use the generic term "eddy-driven" vertical velocity, to refer to the range of (sub)-mesoscale dynamics, i.e. in the scale range 1-100 km. This *eddy pump* of POC could account for 20 to 70% of the local organic carbon export at the base of the euphotic layer (Omand et al., 2015; Stukel, Aluwihare, et al., 2017; Stukel, Song, et al., 2017; Stukel & Ducklow, 2017; Llort et al., 2018), and has been identified as a potential pathway to transfer carbon to depths below the reach of the seasonal mixed-layer (Erickson & Thompson, 2018). Nevertheless, previous observational and fine-scale model estimates of the eddy pump were limited in space and time (typically a few eddy structures over a few weeks/months and the upper 100 m) and excluded the eddy effects on the subduction of DOC. The integrated effect of the eddy pump on the biological carbon pump and its efficiency at exporting carbon to depth are therefore still poorly constrained.

The traditional view that the gravitational pump and mixed-layer pump operate solely on large scales is also being re-assessed. Studies have shown that upward vertical velocities associated with eddies and fronts can supply nutrients to the euphotic zone, locally promote biological production, and eventually modulate the sinking of POC (e.g. Lévy, Ferrari, et al., 2012; Mahadevan, 2016; McGillicuddy, 2016; Harrison et al., 2018). This dynamically driven variability in the gravitational pump could be further re-enforced by biological processes, such as zooplankton diel and seasonal vertical migrations, which are expected to locally add 10% to 200% to the passive sinking flux of POC (Steinberg & Landry, 2017; Jónasdóttir et al., 2015). Eddies and fronts are also known to introduce spatio-temporal variations in the mixed-layer depth, as they can locally re-stratify or de-stratify the water column and modulate the large-scale seasonal patterns in mixed-layer depth (Karleskind et al., 2011; Dufois et al., 2014, 2016; Mahadevan, 2016; Hausmann et al., 2017). Yet, the effect of eddies and fronts on the mixed-layer carbon pump has not been quantified (Hansell et al., 2009; Lévy et al., 2013; Dall'Olmo et al., 2016).

In this study we address some of these open questions. We characterize how the gravitational and physical subduction pumps vary in space and time, quantify how export hotspots occurring at small spatial scales (<100 km) influence the large-scale and seasonal patterns of the export flux, and examine how they might transfer carbon below the euphotic zone and the mixed-layer. We use a high-resolution (2 km) biophysical model of a double-gyre system that captures the mesoscale and part of the sub-mesoscale dynamics (Lévy et al., 2010; Lévy, Iovino, et al., 2012). The model, run over a repeating seasonal cycle, captures the intense frontal and mesoscale activity necessary to represent export hotspots as well as the regional contrasts between the warm low-chlorophyll waters of the subtropical gyre and the cold high-chlorophyll waters of the subpolar gyre (Fig 1, see validation and details in Methods). In the following, section 2 presents the model and how the gravitational, eddy, mixed-layer and Ekman pumps are calculated. In section 3, we examine how the different pumps control the spatial and temporal variability of the organic carbon export flux, and quantify their contribution to the annual export at the base of the euphotic zone and their efficiency at transferring carbon deeper in the water column. Finally, section 4 discusses the implications for measuring and estimating carbon export budgets.



Figure 1. Spatial variability from basin scale to eddy scale over the model’s idealized domain on March 21: A) sea surface temperature (SST), B) surface chlorophyll (SChl), C) mixed-layer depth (MLD) and D) vertical velocity at 100 m depth (W). Upward vertical velocities are positive. Subtropical, jet and subpolar regions are delimited by annual SChl concentrations thresholds of 0.15 and 0.3 mg m^{-3} (black lines) (Resplandy, Martin, et al., 2012). Vertical section S used in Fig 2 is shown in panel B.

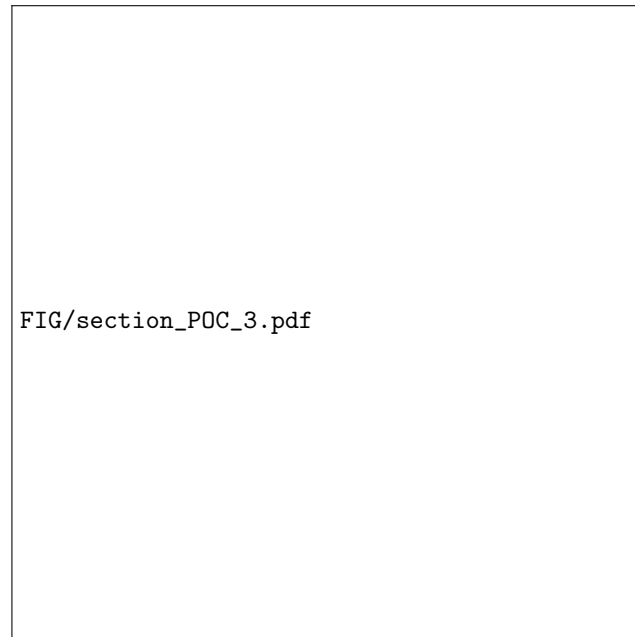


Figure 2. Eddy-driven export hotspots on March 21 along section S (see position in Fig 1 b). a) Model particulate organic carbon (sinking + suspended POC) and vertical velocities (black contours, dashed downwards and solid upwards). b) Model vertical velocities and mixed-layer depth (black). POC export hotspots across the base of the euphotic zone (100 m) are collocated with intensified vertical velocities at frontal regions. Negative velocities are downward. Density contours are indicated in grey.

2 Methods

2.1 Idealized North Atlantic model - description and evaluation

This model is based on the free surface primitive equation ocean model NEMO (Madec, 2008), with 30 z-coordinate vertical layers (10 to 20m in the upper 100m and 300m at the bottom), forced with seasonal zonal profiles of wind, solar radiation, heat and salt fluxes. We used the physical fields of Lévy et al. (Lévy et al., 2010) computed at a horizontal resolution of $1/54^\circ$ (2 km). The spectral analysis of the velocities in this simulation have revealed that the resolved scales are close to $1/9^\circ$ (i.e. ~ 10 km) (Lévy, Resplandy, et al., 2012). Moreover, Lévy, Resplandy, et al. (2012) have shown that the offline advection of a tracer by the velocities computed on a $1/54^\circ$ grid at full resolution or degraded down to $1/9^\circ$ produces patterns that are almost indistinguishable (see their Fig 7). This methodology has the advantage to greatly reduce the numerical cost of the simulation while retaining the strength of the horizontal and vertical velocities produced by the original $1/54^\circ$ model (see details in Lévy, Resplandy, et al., 2012). Therefore, here we used these degraded fields to transport and compute the evolution of the biogeochemical tracers offline.

The biogeochemical module used here is the LOBSTER version described in Resplandy, Lévy, et al. (2012), which includes phytoplankton, zooplankton, semi-labile dissolved organic material (DOM, 5-month time-scale), nitrate, ammonium and 2 classes of sinking detritus (slow and fast sinking rates of 5 m d^{-1} and 200 m d^{-1}). Aggregation and disaggregation of detritus and DOM take into account differential settling and turbulence coagulation mechanisms (Resplandy, Martin, et al., 2012). We use a constant carbon to nitrogen C:N ratio of 6.6 (Redfield proportions) for both POC and DOC. Detailed description and evaluation of the physical and biological dynamics of the model can be found in Lévy et al. (2010); Lévy, Iovino, et al. (2012); Resplandy, Martin, et al. (2012). The spatio-temporal evolution of surface chlorophyll, mixed-layer depth, and surface POC and DOC are shown in supplementary video S1.

The GYRE model reproduces the large-scale distribution of temperature, surface chlorophyll and the particulate export expected from thorium deficit measurements in the North Atlantic (see details in Resplandy, Martin, et al., 2012). It also simulates the features of export hotspots observed in nature. Fig 2 shows three vertical intrusions of POC associated with intensified downward vertical velocities along eddy-driven fronts. These intrusions extend down to 400 m in the model, similar to what has been measured in the North Atlantic (Omand et al., 2015). Finally, the model reproduces subsurface maxima in POC concentrations between the base of the euphotic layer and 600 m (Fig S1), which have been observed *in-situ* and previously used to quantify the strength of the eddy subduction pump (Omand et al., 2015; Stukel, Aluwihare, et al., 2017; Llorc et al., 2018).

Daily maps of the spatial variability in model physical (sea surface temperature, mixed-layer depth, vertical velocity) and biological (Chlorophyll, particulate and dissolved organic carbon concentrations) fields are shown in Figure 1, Figure S2 and Video S1.

2.2 Pumps of organic carbon

For each tracer C (C can be fast sinking POC, slow sinking POC, suspended POC or DOC), the total export E_C is computed off-line as the sum of the gravitational and subduction pumps:

$$E_C = E_{gravitational} + E_{subduction} \quad (1)$$

We further decompose the *subduction pump* into three contributions: the advective flux associated with large-scale Ekman pumping (*Ekman pump*), the eddy-driven advective flux arising from spatio-temporal variations in vertical velocities and organic carbon

(*eddy pump*), and the export associated with vertical mixing (*mixed-layer pump*):

$$E_{subduction} = E_{Ekman} + E_{eddy} + E_{mixed-layer} \quad (2)$$

All terms are computed as a function of depth. Note that in the literature, subduction sometimes includes the mixed-layer pump and the eddy pump (Stukel, Song, et al., 2017), the mixed-layer pump and the Ekman pump (Lévy et al., 2013), or only the eddy pump (Omand et al., 2015).

The *gravitational pump* across the depth level z is computed from the sinking speed V_C of tracer C ($V_C > 0$ for slow and fast sinking POC and $V_C = 0$ for suspended POC and DOC), and the concentration in tracer C at depth z and time-step t ($C(t, z)$):

$$E_{gravitational} = -V_C \times C(t, z) \quad (3)$$

The *Ekman pump* at depth z is computed from the annual mean concentration at depth z ($\overline{C(z)}$) and annual mean vertical velocity at depth z ($\overline{w(z)}$) (overbar indicates the annual average):

$$E_{Ekman} = -\overline{w(z)} \times \overline{C(z)} \quad (4)$$

The *eddy pump* is the residual between the total model vertical advective flux at depth z and time t and the annual Ekman pump at the same depth. It includes spatio-temporal co-variations between vertical velocity $w(t, z)$ and concentrations $C(t, z)$:

$$E_{eddy} = -w(t, z)' \times C(t, z)' \quad (5)$$

with $w(t, z)' = w(t, z) - \overline{w(z)}$ and $C(t, z)' = C(t, z) - \overline{C(z)}$.

The *mixed-layer pump* is often evaluated as a detrainment term assuming an homogeneous concentration of tracer in the mixed-layer (Lévy et al., 2013). Here, however, we use the spatio-temporally varying POC and DOC profiles and simulated vertical diffusivities. Note that using the entrainment method (Lévy et al., 2013) to evaluate the mixed-layer pump is only valid if the mixed-layer is well-mixed (10% in the mixed-layer pump due to the assumption of homogeneity in the mixed-layer). The mixed-layer pump at time t and depth z is computed using the model vertical diffusion coefficient K_z (in $\text{m}^{-2} \text{s}^{-1}$) and the vertical gradient in tracer C :

$$E_{mixed-layer} = K_z(t, z) \times \frac{\partial C(t, z)}{\partial z} \quad (6)$$

These calculations are done from 2-day model average results using a 360-day annual calendar. The seasonal cycle of POC, DOC and the contribution from the different pumps in the subtropical, subpolar and jet regions are shown in Figures S3 and S4. The spatio-temporal evolution of the pumps and the total export of organic carbon are shown in Supplementary Video S2.

For each pump, we compute the probability density distribution of the local export, i.e. at each model point, and the probability density distribution of the export averaged in 100 by 100 km boxes (Fig 4). There are 40,824 points and 551 100km-boxes per time-step in the model domain and 180 time-steps (2-day averaged fields), yielding 7,348,320 local export estimates (Fig 4 a-b) and 99,180 estimates averaged on scales of 100 km (Fig 4 c-d). Monthly maps of the gravitational pump and subduction pump averaged in 100 by 100 km boxes and the spatio-temporal variability of these pumps in these boxes are shown in the Supplementary Material.

3 Results

3.1 Carbon pumps spatial variability at the base of euphotic layer

A starting point for quantifying spatial variability is to consider the daily export flux of total organic carbon (POC + DOC) simulated at the peak of the spring bloom



Figure 3. Export of organic carbon out of the euphotic zone (100 m) in the GYRE model. The total export of DOC and POC comprised of the contributions from the gravitational and subduction pumps. The subduction pump is further decomposed into the mixed-layer, eddy and Ekman pumps. Export contributions are shown on March 21 during the spring bloom (panels a-c and g-i) and averaged annually (panels d-f and j-l). Negative values indicate a downward export and positive values an upward transport.

(here we use March 21). As shown in Fig 3, the total export flux on March 21 shows a basin scale south-to-north gradient strongly modulated by export hotspots (defined here with an arbitrary threshold of local export $> 400 \text{ mgC m}^{-2} \text{ d}^{-1}$). Locally, the export flux on that day can exceed $1000 \text{ mgC m}^{-2} \text{ d}^{-1}$ (up to $4000 \text{ mgC m}^{-2} \text{ d}^{-1}$) and shows variations up to $800 \text{ mgC m}^{-2} \text{ d}^{-1}$ on scales smaller than 100 km.

The background south-to-north gradient in export is largely imposed by the gravitational pump. On March 21, phytoplankton are blooming in the subpolar gyre around 40°N (Fig 1), and the gravitational export is highest on the southern flank of the actively blooming region (30°N to 40°N) due to the 1-2 week lag between the peak in surface phytoplankton and the peak in particle export (Fig 3 b). As previously shown in Resplandy, Martin, et al. (2012), the simulated south-to-north gradient in the gravitational pump falls within the range of values expected from thorium deficit measured during spring and summer in the subtropical, jet and subpolar North Atlantic regions. At smaller scales, hotspots in the gravitational pump are localized in filaments wrapped around eddy structures (Fig 3 b) and mirror the spring bloom patterns delineated by surface Chl and POC concentrations (Figs 1 b and Fig S2). The variability of the gravitational pump in the model is in agreement with high-resolution measurements in the subtropical gyre and jet region that shows variations in the sinking flux on the order of $5\text{-}30 \text{ mgC m}^{-2} \text{ d}^{-1}$ over 40-km transects (see Fig 8 and 10 in Estapa et al., 2015).

Locally, most intense export fluxes are controlled by the subduction pump, and in particular the eddy pump (Fig 3 c, h). The eddy pump follows the patchiness of the vertical velocity field, with hotspots localized at fronts where vertical velocities are larger than 50 m d^{-1} (Fig 1 d). These hotspots can locally re-enforce (negative values), balance, or even reverse (positive values) the export of sinking particles by bringing organic carbon back into the euphotic zone (Fig 3 h). The mixed-layer pump is also patchy (Fig 3 g). On March 21, this pump mostly exports organic carbon in the northern subpolar gyre but modulations of the mixed-layer at spatial scales smaller than 100 km in the jet region (Fig 1 c) locally suppress or enhance the export in specific frontal and mesoscale features.

Fig 4 generalizes the results obtained for March 21 and quantifies how each pump contributes to export hotspots at scales $< 100 \text{ km}$ over the model domain and full seasonal cycle. As suggested by the daily export field, the dynamical spatial variability influences the subduction pump more than the gravitational pump. The eddy pump can locally subduct up to $6000 \text{ mgC m}^{-2} \text{ d}^{-1}$ and upwell up to $4000 \text{ mgC m}^{-2} \text{ d}^{-1}$, the mixed-layer pump can subduct up to $1500 \text{ mgC m}^{-2} \text{ d}^{-1}$, while hotspots in the gravitational pump never exceed $1000 \text{ mgC m}^{-2} \text{ d}^{-1}$ (Fig 4 a, b). Yet, we find that gravitational hotspots are more efficient at exporting organic carbon than subduction hotspots. We evaluate the impact of hotspots on the export at larger scale by comparing the local export (at each model point) with the export averaged over spatial scale of 100-km. The gravitational pump shows no damping of the export flux when averaged over 100-km (similar probability density distribution in Fig 4 a, c). In contrast, subduction hotspots occurring at scales $< 100 \text{ km}$ largely balance when averaged over 100-km areas (tapering of extremes in probability density distribution by a factor 10 from -6000 to $-600 \text{ mgC m}^{-2} \text{ d}^{-1}$, Fig 4 a, c).

In the model, the weak contribution of the eddy pump at spatial scales of 100 km is explained by a strong compensation between downward and upward vertical transport. Although downward hotspots can be larger than upward hotspots (probability density distribution is not symmetric in Fig 4 b), the eddy pump falls below $500 \text{ mgC m}^{-2} \text{ d}^{-1}$ when averaged over spatial scales of 100-km (Fig 4 d). The mixed-layer pump is predominantly exporting carbon downward (negative values, Fig 4 b) but as shown in the daily export flux this pump is patchy and the effect of mixed-layer export hotspots is dampened by contiguous areas of no export (Fig 3 d). As a result,



Figure 4. Export at 100 m depth: a-b) local export at each model point and c-d) averaged over 100 km x 100 km. Gravitational and subduction pumps (left panels) and contributions to subduction from mixed-layer, eddy and Ekman pumps (right panels). Distribution densities are the number of model points (panels a-b) or 100 km x 100 km model boxes (panels c-d) with a certain value of export. The total number of model points is 7,348,320 and the total number of 100 km x 100 km model boxes is 99,180 (see Methods). Monthly maps of the mean export and its spatio-temporal variability in the 100 km x 100 km boxes are shown in Supplementary Material.

the mixed-layer pump also falls below $500 \text{ mgC m}^{-2} \text{ d}^{-1}$ when averaged over spatial scales of 100-km (Fig 4 d).

3.2 Subduction hotspots modulate export seasonal cycle

As shown by three cases studies in Fig 5, the export flux and the contributions from the different pumps also vary in time. On seasonal time-scales, the export is dominated by the gravitational pump and the mixed-layer pump (solid lines indicate average in $100 \times 100 \text{ km}$ areas). The export in the northern subpolar gyre (Box 1) follows the canonical succession of export by the mixed-layer pump in winter and early spring ($200\text{-}300 \text{ mgC m}^{-2} \text{ d}^{-1}$), sinking of particles produced during the spring bloom ($600 \text{ mgC m}^{-2} \text{ d}^{-1}$), followed by a weaker export flux during summer and fall ($100 \text{ mgC m}^{-2} \text{ d}^{-1}$, Fig 5 a-b). The magnitude of this seasonal cycle gradually decreases southward into the jet region (mixed-layer and gravitational pumps $<200 \text{ mgC m}^{-2} \text{ d}^{-1}$ in Box 2, Fig 5 c-d) and disappear in the subtropical gyre (mixed-layer and gravitational pumps $<10 \text{ mgC m}^{-2} \text{ d}^{-1}$ in Box 3, Fig 5 e-f).

On shorter time scales (days to months), the export flux is strongly influenced by the dynamical variability and subduction at small spatial scales. We quantify the impact of spatial variability on the seasonal cycle using the variability of the export flux within the 100-km case study area (shading in Fig 5 is the ± 1 spatial standard deviation in $100 \times 100 \text{ km}$ areas). The eddy pump can locally introduce short-term variations of at least $25\text{-}50 \text{ mgC m}^{-2} \text{ d}^{-1}$ year round in the three areas, and variations as high as $1000 \text{ mgC m}^{-2} \text{ d}^{-1}$ due to specific frontal and eddy features such as the sharp front that passes through box 1 in August/September (Fig 5b and Fig S5). The gravitational and mixed-layer pumps can introduce short-lived variations of $100\text{-}400 \text{ mgC m}^{-2} \text{ d}^{-1}$ in the export flux, but this process is limited in space and time to the subpolar gyre and jet regions during winter and spring (Fig 5 b, d). The patchiness of these two pumps is otherwise weaker and $<50 \text{ mgC m}^{-2} \text{ d}^{-1}$.


3.3 Eddy pump contributes little to annual and regional budgets

On annual average, the export of organic carbon at the base of the euphotic zone is $30 \text{ mgC m}^{-2} \text{ d}^{-1}$ in the subtropical gyre, $70 \text{ mgC m}^{-2} \text{ d}^{-1}$ in the jet region and $120 \text{ mgC m}^{-2} \text{ d}^{-1}$ in the northern subpolar gyre (Fig 3 d, spatial mean over each regions). The gravitational pump accounts for 73% of this annual carbon export over the domain, while the subduction pump in comparison, only accounts for the remaining 27% (Fig 3 e-f, Fig8). The mixed-layer pump alone accounts for 22% of the annual organic carbon export over the domain (i.e. 80% of the subduction pump) but is mostly confined to the subpolar gyre. Despite the presence of strong hotspots, the eddy pump accounts for 4% of the annual export at 100 m at the basin scale, which is similar in magnitude to the contribution of large-scale Ekman pumping found in this study (1%) and derived from global ocean simulations (Levy *et al.*, 2013).

Although the eddy pump and Ekman pump (i.e. advective subduction pumps) contribute little to the annual export over the domain, our results suggest that together these two pumps export more than 60% of the DOC in the jet and subtropical gyre where the mixed-layer pump is weak (Fig 8). This result is consistent with a recent study suggesting that the export of DOC is a major contributor to the export of organic carbon in subtropical gyres (Roshan & DeVries, 2017). Their diagnostic approach does not resolve eddy-driven dynamics and the biological processes producing and decomposing DOC explicitly, but it demonstrates the need for a large export of DOC to reconcile surface DOC production with observed ocean tracer distributions. Our results suggest that subduction could sustain the DOC pump in subtropical gyres inferred by Roshan and DeVries (2017). Finally, we also note that in the subpolar gyre, the Ekman pump yields a weak re-emergence of DOC (upward transport of 5.0



Figure 5. Seasonal and regional variations in export flux at the base of the euphotic zone (100 m depth). The gravitational and subduction pumps (left panels) and individual contributions to the subduction pump (mixed-layer, eddy and Ekman pumps, right panels) are compared in three 100 km x 100 km case studies (Box 1 in subpolar gyre, Box 2 in jet region and Box 3 in subtropical gyre). The mean (solid lines) and the export variability on spatial scales smaller than 100 km (shading indicates ± 1 spatial standard deviation) are shown for each box. The seasonal evolution of DOC and POC in Boxes 1 to 3 is shown in Fig S3, and the export pumps averaged over the subtropical gyre, jet region and subpolar gyre are shown in Fig S4.



FIG/fig_export_depth_POCDOC_log_2panels_May2019_subzdf.pdf

Figure 6. Depth profiles of annual mean export of organic carbon in the subpolar, jet and subtropical regions. Total export sums the gravitational and subduction pumps. The subduction pump is decomposed into contributions from mixed-layer, eddy and Ekman pumps. Box plots of the maximum winter mixed-layer depth are shown (median, 1st and 3rd quartiles, and minimum and maximum values in each region). Export is in log scale.

mgC m⁻² d⁻¹ into the euphotic zone) because of the large DOC export by the mixed-layer pump in winter, which becomes available for upward vertical transport after spring restratification.

3.4 Can the eddy pump transfer carbon deeper in water column?

In the model, the contribution of the subduction pump declines with depth, and at 500 m it only accounts for 2% of the annual organic carbon export, the gravitational pump accounting for the remaining 98% (Tab S1 and Fig S6). Yet, in regions of deep convective winter mixed-layer (such as the northern subpolar gyre in our model), the mixed-layer pump can subduct carbon as deep as 500-1000 m (Fig 6 and Fig S6). In regions of shallower winter mixed-layer (jet and subtropical gyre), the mixed-layer



Figure 7. Eddy pump export (downward transport

<

0 or upward transport

>

0) along randomly picked depth profiles in the model. Mixed-layer depth (black dots) and month of year (colors) are indicated for each profile. Profiles 1 to 5 (thick lines) show eddy pump exporting below the mixed-layer.

pump is limited to the upper 100-200 m but the eddy pump acts as a relay, transferring carbon below the mixed-layer (eddy pump maximum right below the mixed-layer pump maximum in Fig 6 b-c).

The individual depth profiles of the eddy pump shown in Fig 7 suggest its effect is generally confined to the mixed-layer, but can, in some cases, export as much as $500 \text{ mgC m}^{-2} \text{ d}^{-1}$ below the depth of the mixed-layer (e.g. profiles 1 to 5). However, because these events are relatively rare and limited in space and time, their contribution to the annual and regional carbon export is still about 10 times smaller than the gravitational pump (Fig 6). This result is consistent with the study of Stukel, Song, et al. (2017) which showed that, in the California Current, sinking particles were more efficiently exported at depth than subducted particles.

4 Discussion

4.1 Implications and link to *in-situ* measurements

We find that the export of total organic carbon simulated in an idealized double gyre system is highly variable at the eddy scale (that is 100 km and below). Locally,

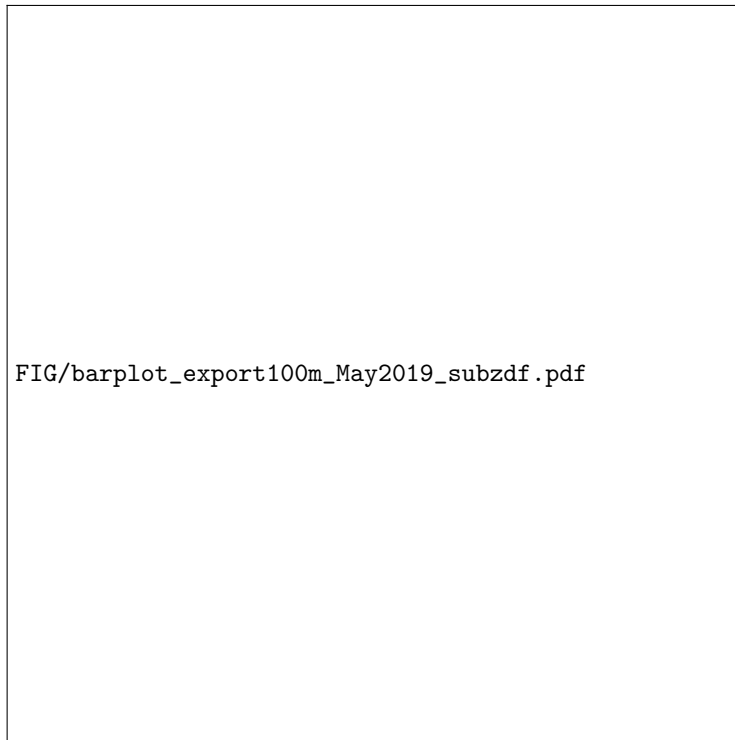


Figure 8. Annual export of DOC and POC (sinking and suspended) at 100 m averaged over the model domain and over the subpolar, jet and subtropical regions. a) Export from the gravitational and subduction pumps and b) contributions to the subduction pump from the mixed-layer, eddy and Ekman pumps. Export fluxes are downward (negative) except for the Ekman pump in the subpolar gyre. Export fluxes are given in Tab S1.

largest export fluxes are sustained by the eddy-driven subduction pump. Simulated hotspots of export up to $1000\text{--}6000 \text{ mgC m}^{-2} \text{ d}^{-1}$ are consistent with previous observations and modeling work focusing on the export along a frontal structure during the subpolar North Atlantic Spring bloom (Omand et al., 2015, see their Fig S12). However, we find that these eddy-driven hotspots contribute less than 5% to the export of organic carbon on annual and regional average. Our model suggests that although hotspots associated with particle sinking (up to $1000 \text{ mgC m}^{-2} \text{ d}^{-1}$) and vertical mixed-layer (up to $1500 \text{ mgC m}^{-2} \text{ d}^{-1}$) are weaker than those of the eddy pump, they are more efficient at exporting carbon.

On annual average and over the domain, the gravitational pump exports 73% and the mixed-layer pump 22% of the total organic carbon. This result appears consistent with the traditional view of the biological pump - dominated by gravitational pump and mixed-layer pump. A major difference however is that in the traditional view, the influence of the mixed-layer pump at the global scale is attributed to the wintertime export of DOC accumulated over the spring and summer seasons (Henson et al., 2012; Hansell et al., 2009), while in our model the mixed-layer pump exports DOC but also large amounts of suspended POC (plankton) at 100 m (Fig 8 b, Tab S1). This downward mixing of suspended POC is associated with eddy-driven sub-seasonal variations in the mixed-layer depth. Short-lived restratification events (time-scale of days) promote not only plankton growth (Mahadevan et al., 2011), but also the export of recently produced suspended POC during the subsequent deepening of the mixed-layer. This efficient mixing of suspended POC accounts for half of the simulated annual subduction pump and about 10-15% of the total export at 100 m depth. This result is supported by recent glider optical observations suggesting that high-frequency vertical mixing of small POC could account for 5-25% of the annual export in the North Atlantic Porcupine Abyssal Plain ($49^{\circ}\text{N}\text{--}16^{\circ}\text{W}$) (Bol et al., 2018). The global export of POC by restratification/destratification was estimated to be $0.1\text{--}0.5 \text{ PgC yr}^{-1}$ using satellite-based POC and float-based mixed-layer depths (Dall’Omo et al., 2016). Our modeling results suggest that heterogeneities in the mixed-layer at small spatial scale play a critical role in sustaining this export of suspended POC.

In our model, eddy pump hotspots are associated with downward eddy-driven vertical velocities larger than 50 m d^{-1} , localized at fronts. These vigorous downward motions are short-lived and compensated by upward velocities. This compensation between upward and downward eddy-driven transport occurs in part at spatial scales of $\sim 100 \text{ km}$ and in part at larger spatial and temporal scales. The compensation between upward and downward transport is however not complete. In line with previous observations and modeling studies (Llort et al., 2018; Stukel, Aluwihare, et al., 2017; Stukel, Song, et al., 2017; Omand et al., 2015), we find that the downward transport of POC across the euphotic layer ($8 \text{ mgC m}^{-2} \text{ d}^{-1}$) exceeds the upward transport of POC ($7 \text{ mgC m}^{-2} \text{ d}^{-1}$) because of the asymmetric effect of upward and downward velocities on the vertical gradient in particles (sharp decline with depth, Fig 2). The integrated effect of eddy-driven POC subduction is however small and accounts for less than 2% of the annual POC export at the regional scale.

This contrasts with the results of a recent study that found very little compensation between upward and downward transports because of a high correlation between high POC concentrations and downward vertical velocities in their model (Omand et al., 2015). In our case, the correlation between high POC values and downward velocities is weak (Pearson correlation coefficient $R = -0.14$ for 150 m POC concentrations $> 15 \text{ mgC m}^{-3}$). A major difference is the more complex biological model used in our study, including nutrients, DOC, phytoplankton, zooplankton and detritus, as well as a representation of the aggregation/fragmentation effect of turbulence and the funneling effect of eddies on detritus (Alldredge et al., 2003; Waite et al., 2016) (see details in SI). The resulting non-linearities temporally decouple production, decay and ex-

port of POC within the evolving 3-D velocity field. In nature, biological processes are more complex than what is represented in any of the models, and whether or not this additional complexity yields more or less coupling between downward velocities and plankton biomass remains to be assessed. A second factor in this comparison, however, is the lower horizontal resolution of our physical model (2 km vs 1 km in Omand et al., 2015), which could yield weaker vertical velocities and underestimate the asymmetry between small-scale upwelling and downwelling across frontal structures (Gula et al., 2014; Mahadevan, 2016).

The magnitude of this compensation between eddy-driven upward and downward carbon transport is difficult to detect and quantify from in-situ observations. Llorca et al. (2018) developed an observation-based method to quantify the eddy-driven subduction of POC in the Southern Ocean, using subsurface maxima in POC detected by biogeochemical floats. By applying the same method to the POC in our model (see Text S1), we find an annual mean POC subduction of $0.6 \text{ mgC m}^{-2} \text{ d}^{-1}$, which represents only a small fraction of the POC downward eddy pump ($8 \text{ mgC m}^{-2} \text{ d}^{-1}$), and about two thirds of the net POC export by the eddy pump (i.e. the sum of downward and upward transport which equals $1 \text{ mgC m}^{-2} \text{ d}^{-1}$, Fig8). The method successfully detected the strong downward subduction events simulated in the jet and subpolar regions, but by design it did not capture the weaker downward export events without POC subsurface signatures nor the upward obduction events (Fig S7). This comparison is however limited by the fact that the model vertical resolution at the subsurface (50-100 m) is lower than the float profile resolution (10-50 m), so the model may underestimate the magnitude of subsurface POC signatures and associated subduction flux. In any case, we note that available observation-based methods to quantify eddy-driven subduction do not detect POC obduction events, and therefore cannot be used to address the compensation of downward and upward POC flux events that we see in our model.

4.2 Caveats and limitations

We acknowledge that there are some caveats in our approach, including the idealized representation of the double gyre system and the biogeochemical and ecosystem dynamics. Observational and modeling studies suggest that the active export of organic carbon by zooplankton vertical migration could add 30 to 50% to the gravitational pump in the North Atlantic (Steinberg & Landry, 2017; Jónasdóttir et al., 2015; Hansen & Visser, 2016), and likely contributes, along with the subduction pump examined here, to the spatial variability in the global biological pump. Zooplankton may also fragment part of the fast sinking large POC into slow sinking small POC and DOC that become more available to microbial respiration (Giering et al., 2014; Baker et al., 2017). Our model includes one class of zooplankton and some parameterization of the fragmentation and aggregation processes of POC linked to the flow turbulence and to zooplankton grazing (Resplandy, Martin, et al., 2012), but does not represent the observed complexity in plankton/microbe dynamics.

Additional factors are the complex spectrum of lability and carbon to nitrogen (C:N) ratios observed in dissolved and particulate organic matter (Amon & Benner, 1994; Hansell, 2013; Hansell & Carlson, 2015). Our model includes a semi-labile DOM pool (remineralisation time-scale of 5 months), which is the pool controlling the seasonal accumulation and carbon export in the ocean (Chap 15 in Hansell & Carlson, 2015). However, our model probably underestimates the size of this pool in the subtropical gyre (observed concentrations of $10 \mu\text{mol C Kg}^{-1}$ (Hansell, 2013) vs. simulated concentrations $<4 \mu\text{mol C Kg}^{-1}$). The model does not include refractory and semi-refractory pools of DOM. Given the temporal and spatial scales considered in this study (≤ 1 year, < 3000 km), refractory DOC has little influence on our results and would correspond to a constant background value equal to deep observed

DOC concentrations ($40 \mu\text{mol Kg}^{-1}$) (Hansell et al., 2009). However, semi-refractory DOC (remineralsation time-scale of years), which accumulates in subtropical gyres ($10 \mu\text{mol Kg}^{-1}$), could enhance export in this region (Hansell, 2013). Finally, our approach ignores spatio-temporal variations in DOM lability and departures in the C:N stoichiometry that could yield a C-enriched DOM and an increased contribution of DOC to the total carbon export. For example, a C:N DOM ratio of 10 would increase the annual DOC export in the subtropical gyre by 50% and the annual carbon export in this region by 10%. Because of the limitations (DOM concentrations, lability and C:N ratio), the relative contribution of DOM to the total export in the subtropical gyre could be larger than simulated in the model. Similarly, our approach does not represent variations in POC lability, which could increase the concentration of small particles and modify the carbon export out of the euphotic zone (Aumont et al., 2017; Baker et al., 2017). These biological processes are known to control the DOC and POC export fields on seasonal to interannual time scales and on regional to basin spatial scales. Nevertheless, their influence on the export at scales < 100 km is still to be determined.

The idealized double gyre physical model used in this study resolves mesoscale eddies but does not fully resolve submesoscale dynamics, which would require a much higher horizontal resolution (McWilliams, 2016). It is therefore likely that the model underestimates vertical velocities and asymmetries in upward and downward transport (Mahadevan, 2016; Gula et al., 2014) and the strength of submesoscale instabilities (Erickson & Thompson, 2018). In addition, the model does not include high-frequency winds, and could therefore underestimate the downward mixing and export of DOC and POC along frontal structures (Whitt et al., 2017). Another related caveat is the offline computation used in our model which filters the impact of internal waves. Recognizing these limitations, we expect the present study to give a lower bound of the export patchiness that can be expected in nature. High-resolution measurements of organic matter dynamics will be key to further constrain the impact of eddy-driven biological-physical interactions on the export flux, test and improve their representation in global and regional models such as the one used here, and refine estimates of the global biological carbon pump.

Acknowledgments

LR is funded by NASA EXPORTS awards 80NSSC17K0555 and NNX16AR50G. DJM gratefully acknowledges support of NSF and NASA grant NNX16AR50G. ML is supported by Centre National d'Etudes Spatiales (CNES) and by the French Agence Nationale de la Recherche award SOBUMPS ANR-16-CE01-0014. The model data are publicly available on Zenodo (zenodo.org/record/3064658.XOWKMpNKhBw) under the DOI:10.5281/zenodo.3064658.

References

- Aldredge, A. L., Granata, T. C., Gotschalk, C. C., & Dickey, T. D. (2003, December). The physical strength of marine snow and its implications for particle disaggregation in the ocean. *Limnology and Oceanography*, *35*(7), 1415–1428. Retrieved 2018-03-30TZ, from <https://aslopubs.onlinelibrary.wiley.com/doi/abs/10.4319/lo.1990.35.7.1415> doi: 10.4319/lo.1990.35.7.1415
- Amon, R. M. W., & Benner, R. (1994, June). Rapid cycling of high-molecular-weight dissolved organic matter in the ocean. *Nature*, *369*(6481), 549. Retrieved 2018-01-19TZ, from <https://www.nature.com/articles/369549a0> doi: 10.1038/369549a0
- Aumont, O., van Hulst, M., Roy-Barman, M., Dutay, J.-C., Éthé, C., & Gehlen, M. (2017, May). Variable reactivity of particulate organic matter in a global ocean biogeochemical model. *Biogeochemistry*, *14*(9), 2321–2341. Retrieved

- 2017-12-13TZ, from <https://www.biogeosciences.net/14/2321/2017/> doi: 10.5194/bg-14-2321-2017
- Baker, C. A., Henson, S. A., Cavan, E. L., Giering, S. L. C., Yool, A., Gehlen, M., ... Sanders, R. (2017, July). Slow-sinking particulate organic carbon in the Atlantic Ocean: Magnitude, flux, and potential controls: Slow-Sinking Particulate Organic Carbon. *Global Biogeochemical Cycles*, *31*(7), 1051–1065. Retrieved 2017-12-13TZ, from <http://doi.wiley.com/10.1002/2017GB005638> doi: 10.1002/2017GB005638
- Benitez-Nelson, C. R., Bidigare, R. R., Dickey, T. D., Landry, M. R., Leonard, C. L., Brown, S. L., ... Yang, E. J. (2007, May). Mesoscale Eddies Drive Increased Silica Export in the Subtropical Pacific Ocean. *Science*, *316*(5827), 1017–1021. Retrieved 2017-10-20TZ, from <http://science.sciencemag.org/content/316/5827/1017> doi: 10.1126/science.1136221
- Bol, R., Henson, S., Anne, Rumyantseva, A., & Briggs, N. (2018, December). High-frequency variability of small-particle carbon export flux in the Northeast Atlantic. *Global Biogeochemical Cycles*, 2018GB005963. Retrieved 2019-05-17TZ, from <https://onlinelibrary.wiley.com/doi/abs/10.1029/2018GB005963> doi: 10.1029/2018GB005963
- Bopp, L., Resplandy, L., Orr, J. C., Doney, S. C., Dunne, J. P., Gehlen, M., ... Vichi, M. (2013, October). Multiple stressors of ocean ecosystems in the 21st century: projections with CMIP5 models. *Biogeosciences*, *10*(10), 6225–6245. Retrieved 2015-03-31TZ, from <http://www.biogeosciences.net/10/6225/2013/> doi: 10.5194/bg-10-6225-2013
- Boyd, P. W., Claustre, H., Levy, M., Siegel, D. A., & Weber, T. (2019, April). Multi-faceted particle pumps drive carbon sequestration in the ocean. *Nature*, *568*(7752), 327–335. Retrieved 2019-05-13TZ, from <http://www.nature.com/articles/s41586-019-1098-2> doi: 10.1038/s41586-019-1098-2
- Boyd, P. W., & Trull, T. W. (2007, March). Understanding the export of biogenic particles in oceanic waters: Is there consensus? *Progress in Oceanography*, *72*(4), 276–312. Retrieved 2017-11-28TZ, from <http://www.sciencedirect.com/science/article/pii/S0079661106001340> doi: 10.1016/j.pocean.2006.10.007
- Buesseler, K., Pike, S., Maiti, K., Lamborg, C., Siegel, D., & Trull, T. (2009, July). Thorium-234 as a tracer of spatial, temporal and vertical variability in particle flux in the North Pacific. *Deep Sea Research Part I: Oceanographic Research Papers*, *56*(7), 1143–1167. Retrieved 2018-05-14TZ, from <http://linkinghub.elsevier.com/retrieve/pii/S0967063709000715> doi: 10.1016/j.dsr.2009.04.001
- Dall’Olmo, G., Dingle, J., Polimene, L., Brewin, R. J. W., & Claustre, H. (2016, November). Substantial energy input to the mesopelagic ecosystem from the seasonal mixed-layer pump. *Nature Geoscience*, *9*(11), 820–823. Retrieved 2018-10-04TZ, from <https://www.nature.com/articles/ngeo2818> doi: 10.1038/ngeo2818
- DeVries, T., & Weber, T. (2017, March). The export and fate of organic matter in the ocean: New constraints from combining satellite and oceanographic tracer observations. *Global Biogeochemical Cycles*, *31*(3), 2016GB005551. Retrieved from <http://onlinelibrary.wiley.com/doi/10.1002/2016GB005551/abstract> doi: 10.1002/2016GB005551
- Dufois, F., Hardman-Mountford, N. J., Greenwood, J., Richardson, A. J., Feng, M., & Matear, R. J. (2016, May). Anticyclonic eddies are more productive than cyclonic eddies in subtropical gyres because of winter mixing. *Science Advances*, *2*(5), e1600282. Retrieved 2018-03-27TZ, from <http://advances.sciencemag.org/content/2/5/e1600282> doi: 10.1126/sciadv.1600282
- Dufois, F., Hardman-Mountford, N. J., Greenwood, J., Richardson, A. J., Feng,

- M., Herbette, S., & Matear, R. (2014, November). Impact of eddies on surface chlorophyll in the South Indian Ocean. *Journal of Geophysical Research: Oceans*, *119*(11), 8061–8077. Retrieved 2018-03-27TZ, from <https://agupubs.onlinelibrary.wiley.com/doi/abs/10.1002/2014JC010164> doi: 10.1002/2014JC010164
- Dunne, J. P., Sarmiento, J. L., & Gnanadesikan, A. (2007, December). A synthesis of global particle export from the surface ocean and cycling through the ocean interior and on the seafloor. *Global Biogeochemical Cycles*, *21*(4), GB4006. Retrieved 2016-02-08TZ, from <http://onlinelibrary.wiley.com/doi/10.1029/2006GB002907/abstract> doi: 10.1029/2006GB002907
- Erickson, Z. K., & Thompson, A. F. (2018). The Seasonality of Physically Driven Export at Submesoscales in the Northeast Atlantic Ocean. *Global Biogeochemical Cycles*, *32*(0). Retrieved 2018-08-16TZ, from <https://agupubs.onlinelibrary.wiley.com/doi/abs/10.1029/2018GB005927> doi: 10.1029/2018GB005927
- Estapa, M. L., Siegel, D. A., Buesseler, K. O., Stanley, R. H. R., Lomas, M. W., & Nelson, N. B. (2015, August). Decoupling of net community and export production on submesoscales in the Sargasso Sea. *Global Biogeochemical Cycles*, *29*(8), 2014GB004913. Retrieved 2017-09-29TZ, from <http://onlinelibrary.wiley.com/doi/10.1002/2014GB004913/abstract> doi: 10.1002/2014GB004913
- Falkowski, P. G., Barber, R. T., & Smetacek, V. (1998, July). Biogeochemical Controls and Feedbacks on Ocean Primary Production. *Science*, *281*(5374), 200–206. Retrieved 2018-01-23TZ, from <http://science.sciencemag.org/content/281/5374/200> doi: 10.1126/science.281.5374.200
- Giering, S. L. C., Sanders, R., Lampitt, R. S., Anderson, T. R., Tamburini, C., Boutrif, M., ... Mayor, D. J. (2014, March). Reconciliation of the carbon budget in the ocean's twilight zone. *Nature*, *507*(7493), 480. Retrieved 2018-01-18TZ, from <https://www.nature.com/articles/nature13123> doi: 10.1038/nature13123
- Guidi, L., Calil, P. H. R., Duhamel, S., Björkman, K. M., Doney, S. C., Jackson, G. A., ... Karl, D. M. (2012, June). Does eddy-eddy interaction control surface phytoplankton distribution and carbon export in the North Pacific Subtropical Gyre? *Journal of Geophysical Research: Biogeosciences*, *117*(G02024). Retrieved 2015-04-01TZ, from <http://doi.wiley.com/10.1029/2012JG001984> doi: 10.1029/2012JG001984
- Gula, J., Molemaker, M. J., & McWilliams, J. C. (2014, July). Submesoscale Cold Filaments in the Gulf Stream. *Journal of Physical Oceanography*, *44*(10), 2617–2643. Retrieved 2018-04-30TZ, from <https://journals.ametsoc.org/doi/abs/10.1175/JPO-D-14-0029.1> doi: 10.1175/JPO-D-14-0029.1
- Hansell, D. A. (2013). Recalcitrant Dissolved Organic Carbon Fractions. *Annual Review of Marine Science*, *5*(1), 421–445. Retrieved 2018-01-19TZ, from <https://doi.org/10.1146/annurev-marine-120710-100757> doi: 10.1146/annurev-marine-120710-100757
- Hansell, D. A., & Carlson, C. A. (Eds.). (2015). *Biogeochemistry of Marine Dissolved Organic Matter (Second Edition)*. Boston: Academic Press. Retrieved 2017-05-17TZ, from <http://www.sciencedirect.com/science/article/pii/B9780124059405099945> doi: 10.1016/B978-0-12-405940-5.09994-5
- Hansell, D. A., Carlson, C. A., Repeta, D. J., & Schlitzer, R. (2009). Dissolved organic matter in the ocean: A controversy stimulates new insights. *Oceanography*, *22*(4). Retrieved 2017-05-17TZ, from <https://darchive.mblwhoilibrary.org/handle/1912/3183>
- Hansen, A. N., & Visser, A. W. (2016, January). Carbon export by vertically migrating zooplankton: an optimal behavior model. *Limnology and Oceanography*, *61*(2), 701–710. Retrieved 2018-03-30TZ, from <https://>

- aslopubs.onlinelibrary.wiley.com/doi/abs/10.1002/lno.10249 doi: 10.1002/lno.10249
- Harrison, C. S., Long, M. C., Lovenduski, N. S., & Moore, J. K. (2018). Mesoscale Effects on Carbon Export: A Global Perspective. *Global Biogeochemical Cycles*, *32*. Retrieved 2018-04-30TZ, from <https://agupubs.onlinelibrary.wiley.com/doi/abs/10.1002/2017GB005751> doi: 10.1002/2017GB005751
- Hausmann, U., McGillicuddy, D. J., & Marshall, J. (2017, January). Observed mesoscale eddy signatures in Southern Ocean surface mixed-layer depth. *Journal of Geophysical Research: Oceans*, *122*(1), 617–635. Retrieved 2018-03-27TZ, from <https://agupubs.onlinelibrary.wiley.com/doi/abs/10.1002/2016JC012225> doi: 10.1002/2016JC012225
- Henson, S. A., Sanders, R., & Madsen, E. (2012, March). Global patterns in efficiency of particulate organic carbon export and transfer to the deep ocean. *Global Biogeochemical Cycles*, *26*(1), GB1028. Retrieved from <http://onlinelibrary.wiley.com/doi/10.1029/2011GB004099/abstract> doi: 10.1029/2011GB004099
- Henson, S. A., Sanders, R., Madsen, E., Morris, P. J., Le Moigne, F., & Quartly, G. D. (2011, February). A reduced estimate of the strength of the ocean's biological carbon pump. *Geophysical Research Letters*, *38*(4), L04606. Retrieved from <http://onlinelibrary.wiley.com/doi/10.1029/2011GL046735/abstract> doi: 10.1029/2011GL046735
- Jónasdóttir, S. H., Visser, A. W., Richardson, K., & Heath, M. R. (2015, September). Seasonal copepod lipid pump promotes carbon sequestration in the deep North Atlantic. *Proceedings of the National Academy of Sciences*, *112*(39), 12122–12126. Retrieved 2017-12-13TZ, from <http://www.pnas.org/content/112/39/12122> doi: 10.1073/pnas.1512110112
- Karleskind, P., Lévy, M., & Memery, L. (2011, February). Subduction of carbon, nitrogen, and oxygen in the northeast Atlantic. *Journal of Geophysical Research*, *116*(C2). Retrieved 2015-04-01TZ, from <http://doi.wiley.com/10.1029/2010JC006446> doi: 10.1029/2010JC006446
- Laws, E. A., Falkowski, P. G., Smith, W. O., Ducklow, H., & McCarthy, J. J. (2000, December). Temperature effects on export production in the open ocean. *Global Biogeochemical Cycles*, *14*(4), 1231–1246. Retrieved 2017-11-28TZ, from <http://onlinelibrary.wiley.com/doi/10.1029/1999GB001229/abstract> doi: 10.1029/1999GB001229
- Llort, J., Langlais C., Matear R., Moreau S., Lenton A., & Strutton Peter G. (2018, February). Evaluating Southern Ocean Carbon Eddy-Pump From Biogeochemical-Argo Floats. *Journal of Geophysical Research: Oceans*, *123*(2), 971–984. Retrieved 2018-03-27TZ, from <https://agupubs.onlinelibrary.wiley.com/doi/full/10.1002/2017JC012861> doi: 10.1002/2017JC012861
- Lévy, M., Bopp, L., Karleskind, P., Resplandy, L., Ethe, C., & Pinsard, F. (2013, December). Physical pathways for carbon transfers between the surface mixed layer and the ocean interior. *Global Biogeochemical Cycles*, *27*(4), 1001–1012. Retrieved 2015-03-31TZ, from <http://doi.wiley.com/10.1002/gbc.20092> doi: 10.1002/gbc.20092
- Lévy, M., Ferrari, R., Franks, P. J. S., Martin, A. P., & Rivière, P. (2012, July). Bringing physics to life at the submesoscale: FRONTIER. *Geophysical Research Letters*, *39*(14), n/a–n/a. Retrieved 2015-04-01TZ, from <http://doi.wiley.com/10.1029/2012GL052756> doi: 10.1029/2012GL052756
- Lévy, M., Iovino, D., Resplandy, L., Klein, P., Madec, G., Tréguier, A.-M., ... Takahashi, K. (2012, January). Large-scale impacts of submesoscale dynamics on phytoplankton: Local and remote effects. *Ocean Modelling*, *43-44*, 77–93. Retrieved 2015-03-31TZ, from <http://linkinghub.elsevier.com/retrieve/pii/S1463500311002009> doi: 10.1016/j.ocemod.2011.12.003
- Lévy, M., Klein, P., & Treguier, A.-M. (2001). Impact of sub-mesoscale physics

- on production and subduction of phytoplankton in an oligotrophic regime. *Journal of marine research*, 59(4), 535–565. Retrieved 2015-04-01TZ, from <http://www.ingentaconnect.com/content/jmr/jmr/2001/00000059/00000004/art00003>
- Lévy, M., Klein, P., Tréguier, A.-M., Iovino, D., Madec, G., Masson, S., & Takahashi, K. (2010, January). Modifications of gyre circulation by sub-mesoscale physics. *Ocean Modelling*, 34(1-2), 1–15. Retrieved 2015-04-01TZ, from <http://linkinghub.elsevier.com/retrieve/pii/S1463500310000582> doi: 10.1016/j.ocemod.2010.04.001
- Lévy, M., Resplandy, L., Klein, P., Capet, X., Iovino, D., & Ethé, C. (2012, May). Grid degradation of submesoscale resolving ocean models: Benefits for offline passive tracer transport. *Ocean Modelling*, 48, 1–9. Retrieved 2015-03-31TZ, from <http://linkinghub.elsevier.com/retrieve/pii/S1463500312000340> doi: 10.1016/j.ocemod.2012.02.004
- Madec, G. (2008). *NEMO ocean engine*. Note du Pôle de modélisation, Institut Pierre-Simon Laplace (IPSL), France, No 27, ISSN No 1288-1619.
- Mahadevan, A. (2016). The Impact of Submesoscale Physics on Primary Productivity of Plankton. *Annual Review of Marine Science*, 8(1), 161–184. Retrieved 2016-01-25TZ, from <http://dx.doi.org/10.1146/annurev-marine-010814-015912> doi: 10.1146/annurev-marine-010814-015912
- Mahadevan, A., Tagliabue, A., Bopp, L., Lenton, A., Memery, L., & Levy, M. (2011, May). Impact of episodic vertical fluxes on sea surface pCO₂. *Philosophical Transactions of the Royal Society A: Mathematical, Physical and Engineering Sciences*, 369(1943), 2009–2025. Retrieved 2015-04-01TZ, from <http://rsta.royalsocietypublishing.org/cgi/doi/10.1098/rsta.2010.0340> doi: 10.1098/rsta.2010.0340
- McGillicuddy, D. J. (2016). Mechanisms of Physical-Biological-Biogeochemical Interaction at the Oceanic Mesoscale. *Annual Review of Marine Science*, 8(1), 125–159. Retrieved 2017-03-29TZ, from <http://dx.doi.org/10.1146/annurev-marine-010814-015606> doi: 10.1146/annurev-marine-010814-015606
- McGillicuddy, D. J., Anderson, L. A., Bates, N. R., Bibby, T., Buesseler, K. O., Carlson, C. A., ... Steinberg, D. K. (2007, May). Eddy/Wind Interactions Stimulate Extraordinary Mid-Ocean Plankton Blooms. *Science*, 316(5827), 1021–1026. Retrieved 2017-10-26TZ, from <http://science.sciencemag.org/content/316/5827/1021> doi: 10.1126/science.1136256
- McWilliams, J. C. (2016, May). Submesoscale currents in the ocean. *Proc. R. Soc. A*, 472(2189), 20160117. Retrieved 2017-12-04TZ, from <http://rspa.royalsocietypublishing.org/content/472/2189/20160117> doi: 10.1098/rspa.2016.0117
- Newton, P. P., Lampitt, R. S., Jickells, T. D., King, P., & Boutle, C. (1994, November). Temporal and spatial variability of biogenic particles fluxes during the JGOFS northeast Atlantic process studies at 47n, 20w. *Deep Sea Research Part I: Oceanographic Research Papers*, 41(11), 1617–1642. Retrieved 2018-11-05TZ, from <http://www.sciencedirect.com/science/article/pii/0967063794900655> doi: 10.1016/0967-0637(94)90065-5
- Omand, M. M., D’Asaro, E. A., Lee, C. M., Perry, M. J., Briggs, N., Cetinić, I., & Mahadevan, A. (2015, April). Eddy-driven subduction exports particulate organic carbon from the spring bloom. *Science*, 348(6231), 222–225. Retrieved 2017-05-30TZ, from <http://science.sciencemag.org/content/348/6231/222> doi: 10.1126/science.1260062
- Resplandy, L., Lévy, M., Bopp, L., Echevin, V., Pous, S., Sarma, V. V. S. S., & Kumar, D. (2012, December). Controlling factors of the oxygen balance in the Arabian Sea’s OMZ. *Biogeosciences*, 9(12), 5095–5109. Retrieved 2015-03-31TZ, from <http://www.biogeosciences.net/9/5095/2012/> doi: 10.5194/bg-9-5095-2012

- Resplandy, L., Martin, A., Le Moigne, F., Martin, P., Aquilina, A., Mémery, L., ... Sanders, R. (2012, October). How does dynamical spatial variability impact 234th-derived estimates of organic export? *Deep Sea Research Part I: Oceanographic Research Papers*, 68, 24–45. Retrieved 2015-03-31TZ, from <http://linkinghub.elsevier.com/retrieve/pii/S0967063712001343> doi: 10.1016/j.dsr.2012.05.015
- Roshan, S., & DeVries, T. (2017, December). Efficient dissolved organic carbon production and export in the oligotrophic ocean. *Nature Communications*, 8(1), 2036. Retrieved 2017-12-13TZ, from <https://www.nature.com/articles/s41467-017-02227-3> doi: 10.1038/s41467-017-02227-3
- Schlitzer, R. (2004). Export production in the equatorial and North Pacific derived from dissolved oxygen, nutrient and carbon data. *Journal of Oceanography*, 60(1), 53–62. Retrieved 2017-07-03TZ, from <http://www.springerlink.com/index/UL2015445P4TN046.pdf>
- Siegel, D. A., Buesseler, K. O., Doney, S. C., Sailley, S. F., Behrenfeld, M. J., & Boyd, P. W. (2014, March). Global assessment of ocean carbon export by combining satellite observations and food-web models. *Global Biogeochemical Cycles*, 28(3), 181–196. Retrieved 2017-07-10TZ, from <http://doi.wiley.com/10.1002/2013GB004743> doi: 10.1002/2013GB004743
- Steinberg, D. K., & Landry, M. R. (2017). Zooplankton and the Ocean Carbon Cycle. *Annual Review of Marine Science*, 9(1), 413–444. Retrieved 2017-09-29TZ, from <https://doi.org/10.1146/annurev-marine-010814-015924> doi: 10.1146/annurev-marine-010814-015924
- Stukel, M. R., Aluwihare, L. I., Barbeau, K. A., Chekalyuk, A. M., Goericke, R., Miller, A. J., ... Landry, M. R. (2017, February). Mesoscale ocean fronts enhance carbon export due to gravitational sinking and subduction. *Proceedings of the National Academy of Sciences*, 114(6), 1252–1257. Retrieved 2017-12-07TZ, from <http://www.pnas.org/lookup/doi/10.1073/pnas.1609435114> doi: 10.1073/pnas.1609435114
- Stukel, M. R., & Ducklow, H. W. (2017, September). Stirring Up the Biological Pump: Vertical Mixing and Carbon Export in the Southern Ocean. *Global Biogeochemical Cycles*, 31(9), 2017GB005652. Retrieved 2017-10-13TZ, from <http://onlinelibrary.wiley.com/doi/10.1002/2017GB005652/abstract> doi: 10.1002/2017GB005652
- Stukel, M. R., Song, H., Goericke, R., & Miller, A. J. (2017). The role of subduction and gravitational sinking in particle export, carbon sequestration, and the remineralization length scale in the California Current Ecosystem: Subduction and sinking particle export in the CCE. *Limnology and Oceanography*, 63(1), 363–383. Retrieved 2018-01-23TZ, from <http://doi.wiley.com/10.1002/lno.10636> doi: 10.1002/lno.10636
- Waite, A. M., Stemmann, L., Guidi, L., Calil, P. H. R., Hogg, A. M. C., Feng, M., ... Gorsky, G. (2016, September). The wineglass effect shapes particle export to the deep ocean in mesoscale eddies. *Geophysical Research Letters*, 43(18), 2015GL066463. Retrieved 2017-03-29TZ, from <http://onlinelibrary.wiley.com/doi/10.1002/2015GL066463/abstract> doi: 10.1002/2015GL066463
- Whitt, D. B., Lévy, M., & Taylor, J. R. (2017, February). Low-frequency and high-frequency oscillatory winds synergistically enhance nutrient entrainment and phytoplankton at fronts. *Journal of Geophysical Research: Oceans*, 122(2), 1016–1041. Retrieved 2018-04-26TZ, from <https://agupubs.onlinelibrary.wiley.com/doi/abs/10.1002/2016JC012400> doi: 10.1002/2016JC012400

Figure 1.

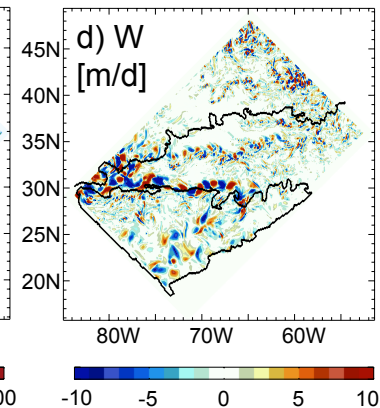
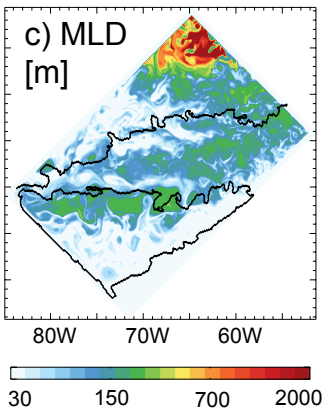
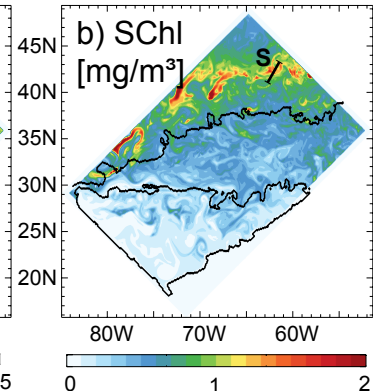
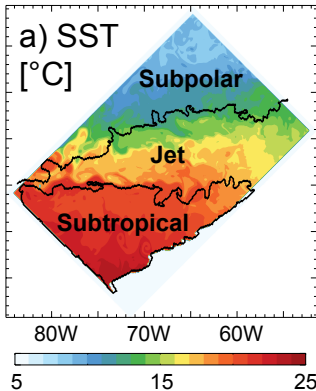
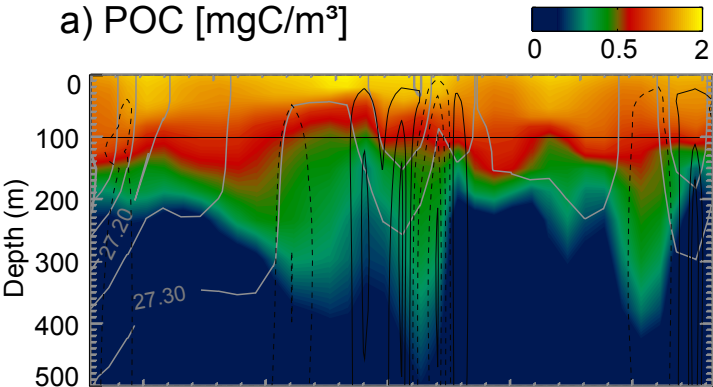


Figure 2.

a) POC [mgC/m³]



b) Vertical velocities [m/d]

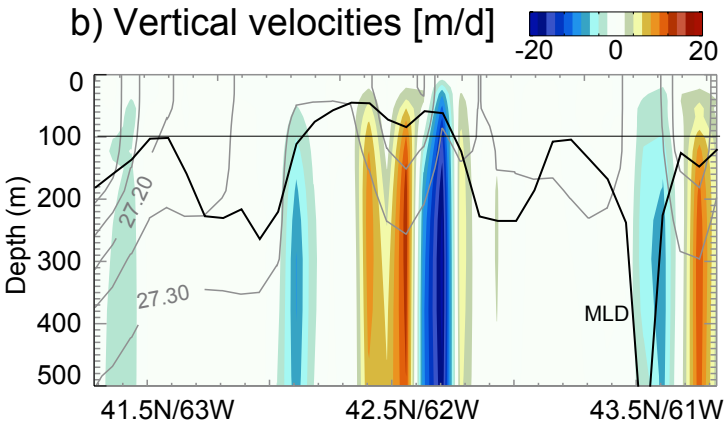
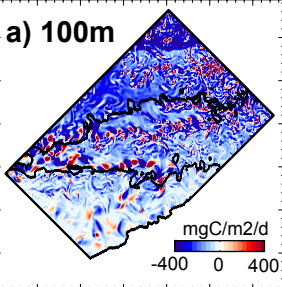
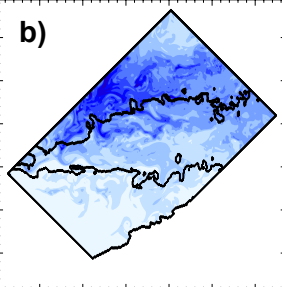


Figure 3.

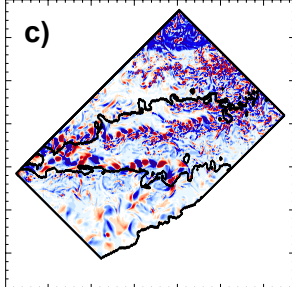
Total Export



100 m depth Gravitational Pump

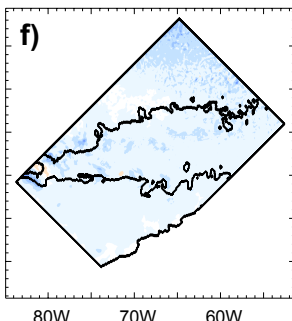
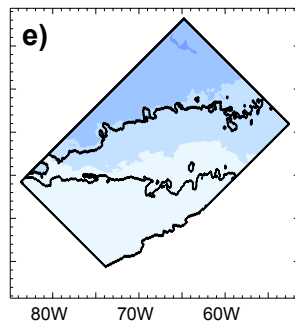
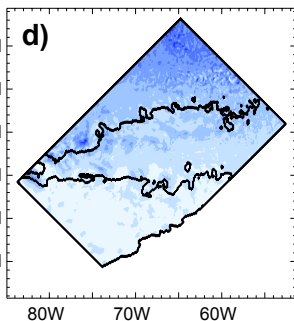


Subduction Pump



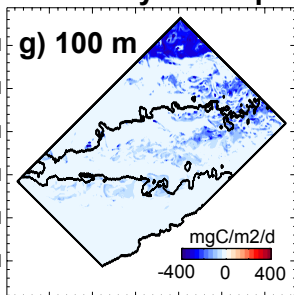
March 21

Annual mean

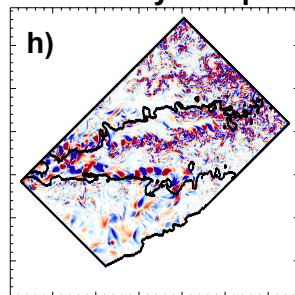


Subduction contributions

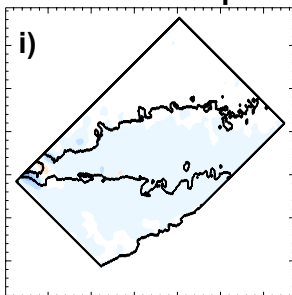
Mixed-layer Pump



Eddy Pump



Ekman Pump



March 21

Annual mean

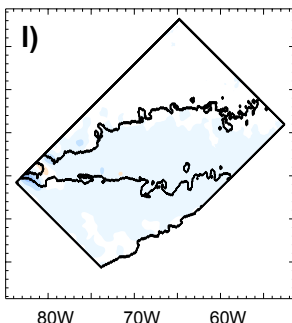
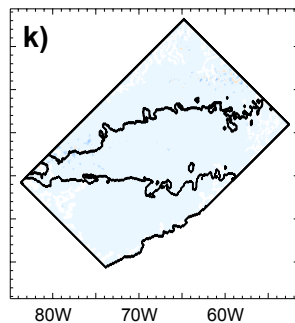
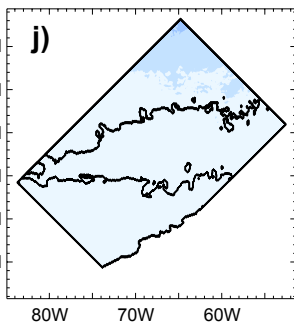


Figure 4.

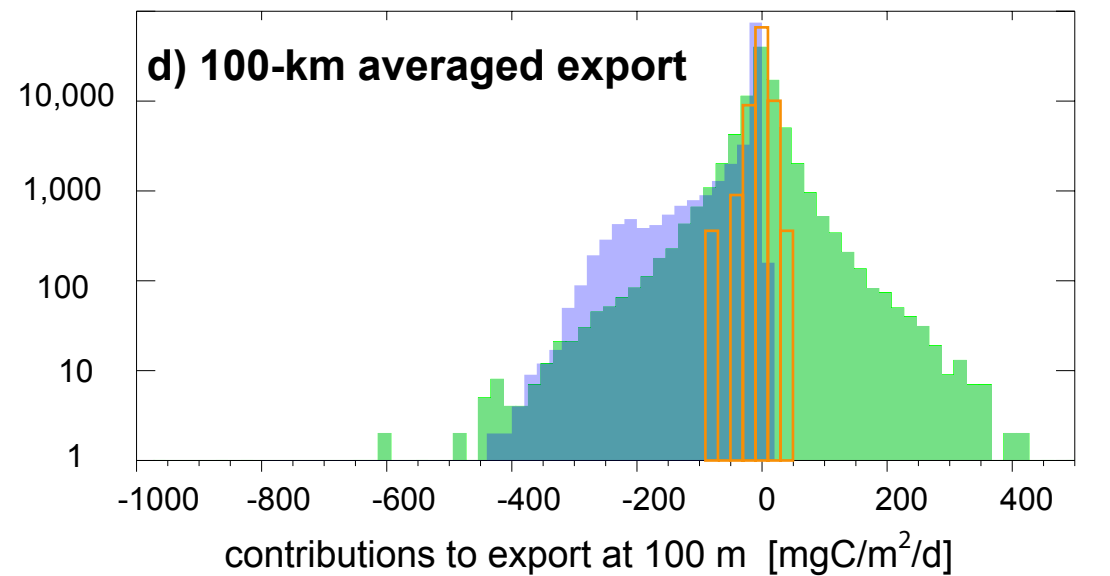
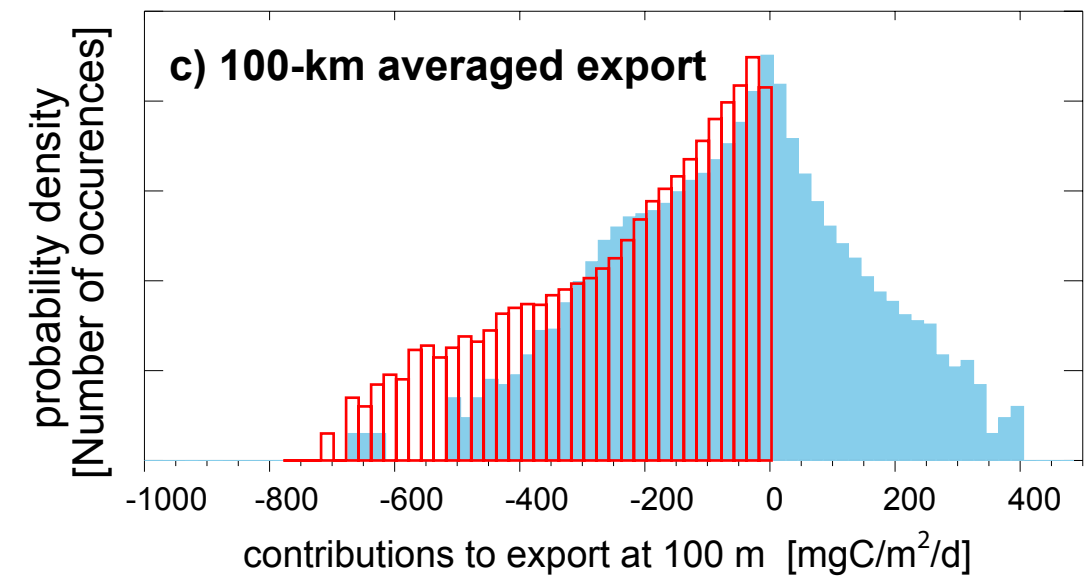
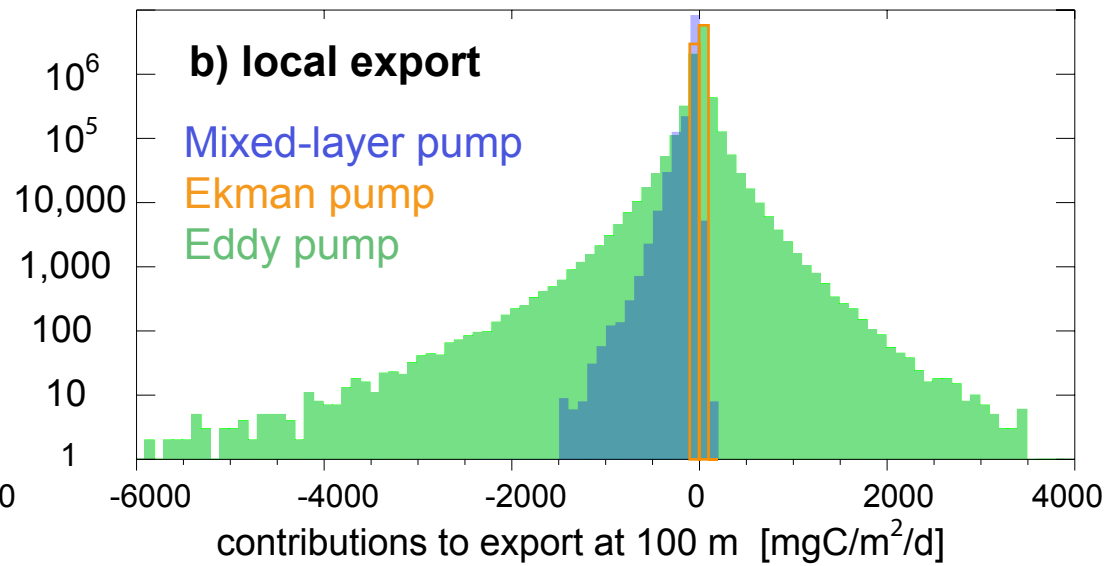
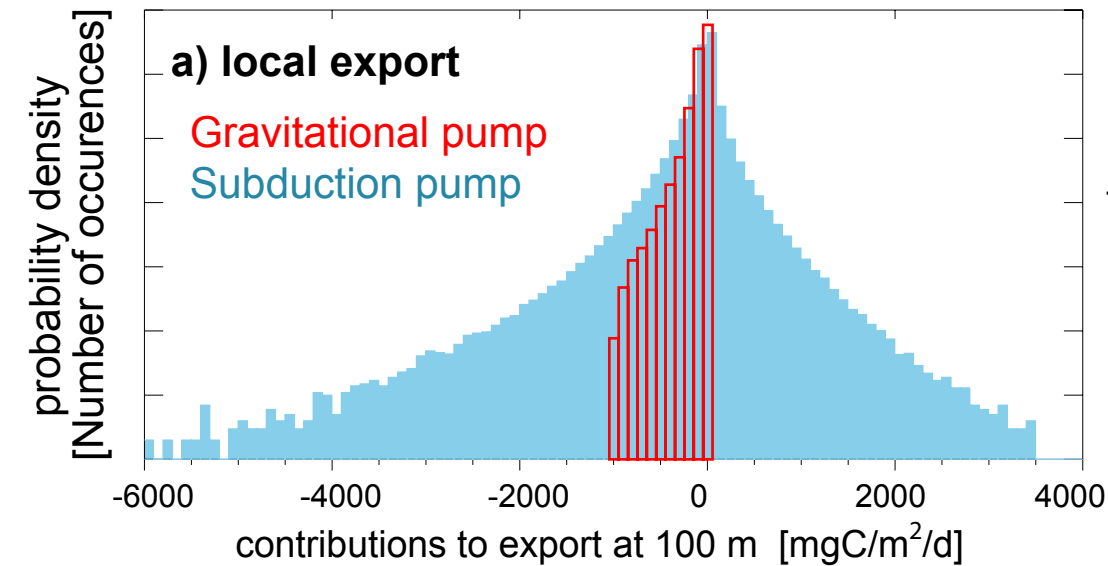


Figure 5.

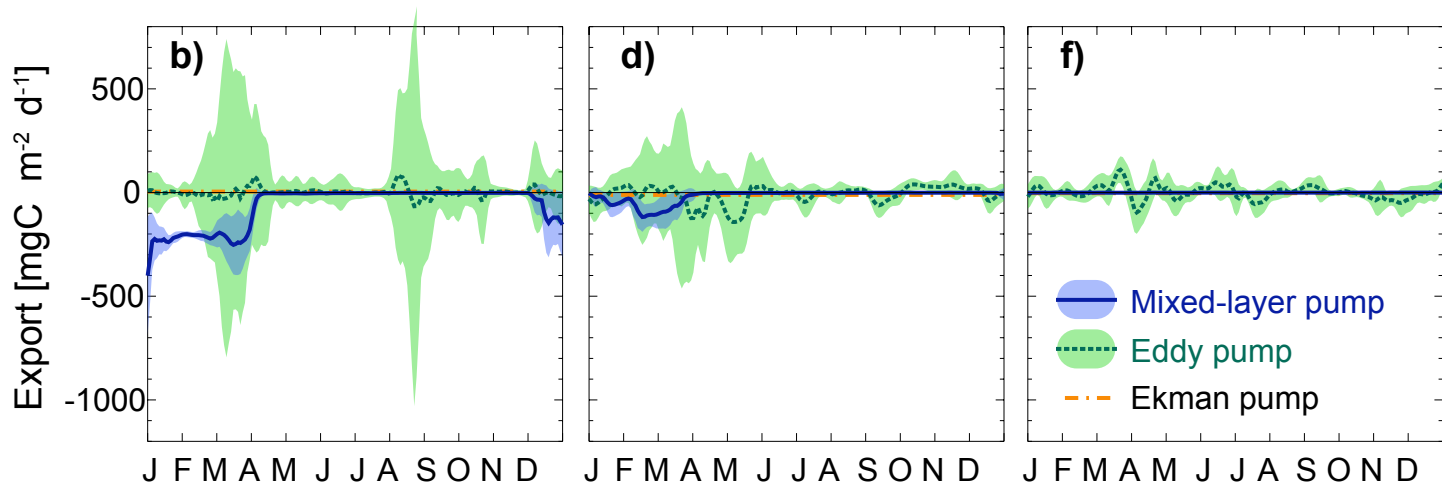
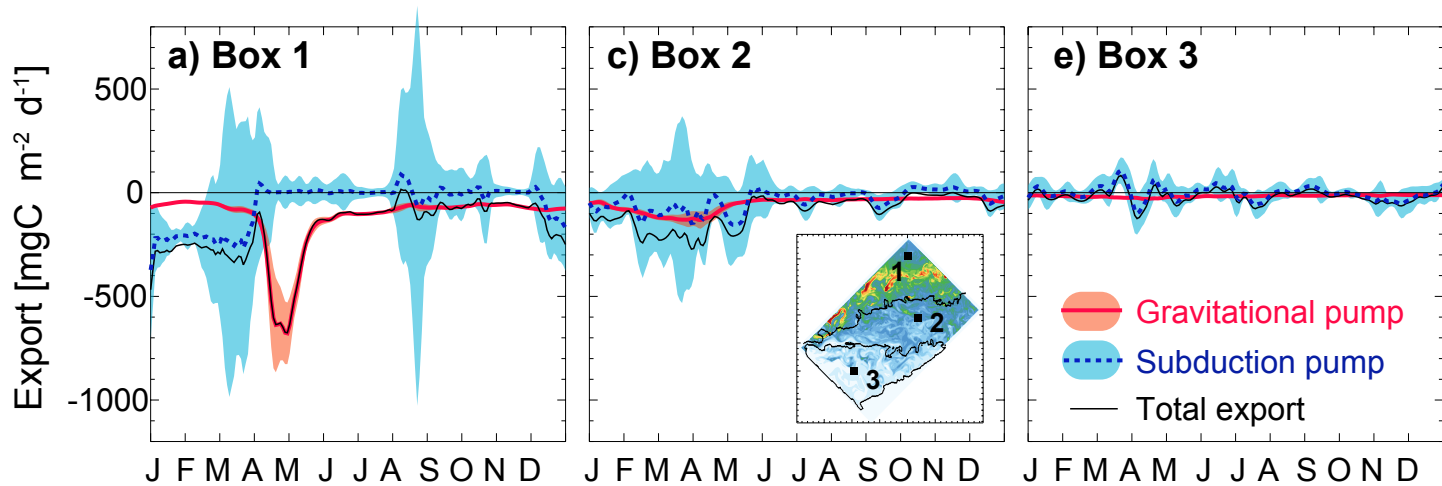


Figure 6.

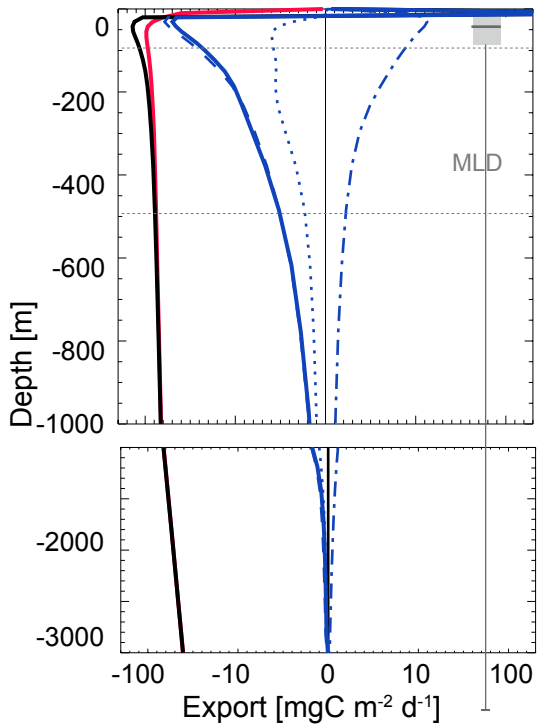
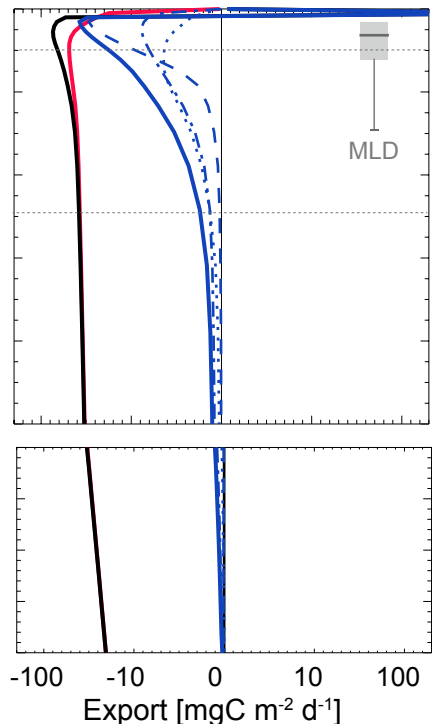
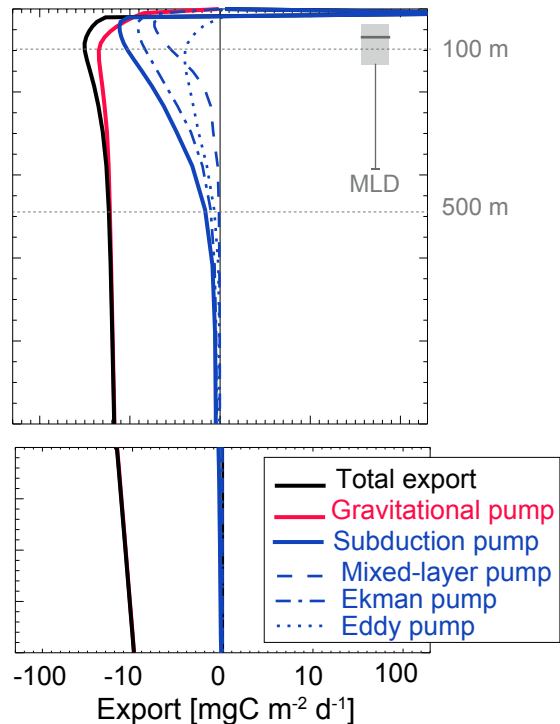
a) Subpolar gyre**b) Jet region****c) Subtropical gyre**

Figure 7.

Eddy Pump

← - 500 mgC m⁻² d⁻¹

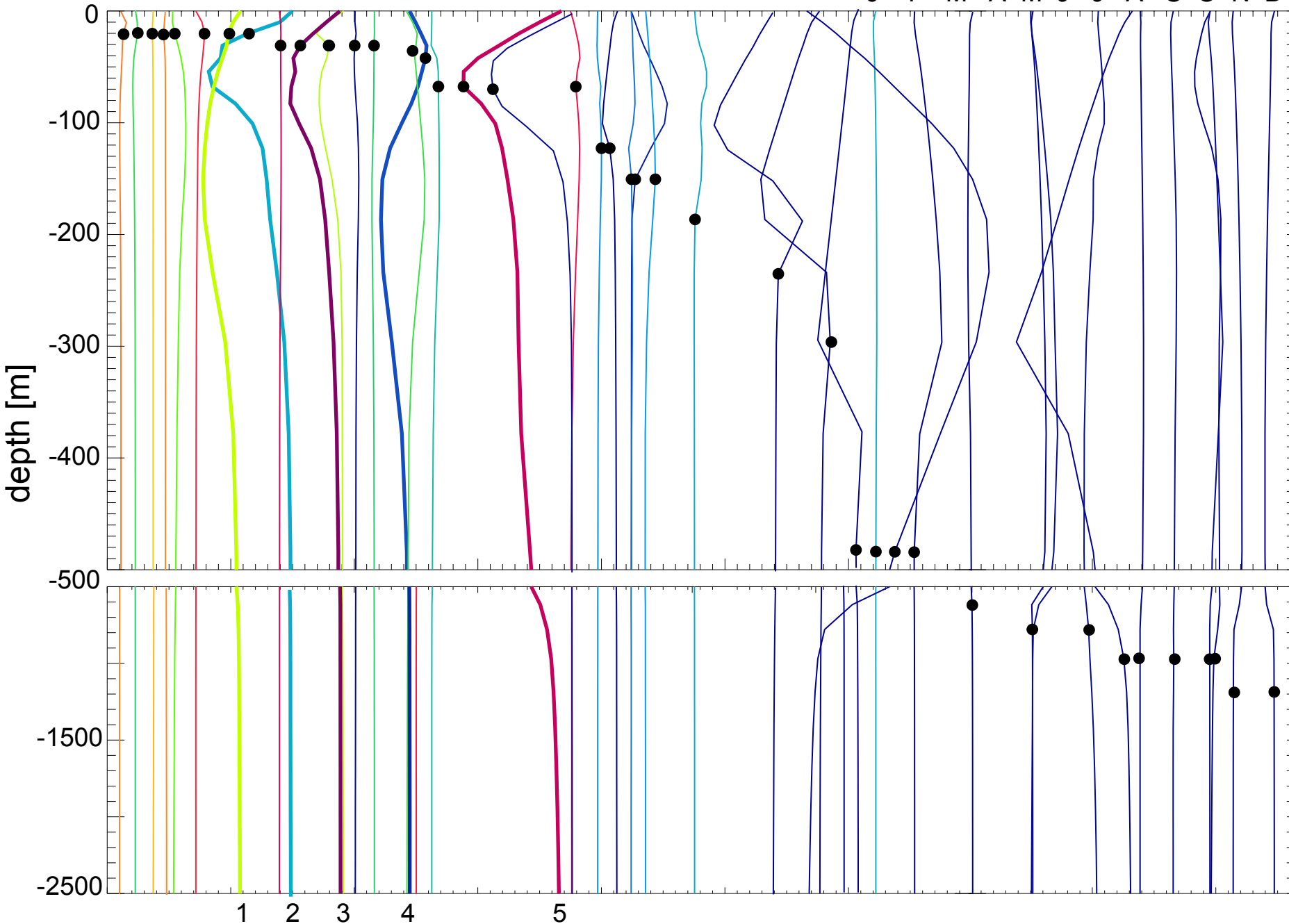


Figure 8.

